Determination of the Optimal Battery Capacity of a Grid-connected Photovoltaic System with Power and Frequency Fluctuations Consideration

Chattrin Thongsawaeng[*1] and **Kulyos Audomvongseree**[*2], Non-members

ABSTRACT

Power and frequency fluctuations are main problems of a grid-connected photovoltaic (PV) system. To effectively remedy this problem, appropriate size of battery should be installed into the PV system. In this paper, the dynamic model of the photovoltaic system and battery are discussed. The battery used in this analysis is lead-acid battery. In addition, the dependent structure of solar irradiance and ambient temperature are taken into account. The proposed algorithm begins with solar radiation-temperature model. Then, the output power of the PV system will be calculated based on the PV dynamic model. The rest of the interconnected power system is modeled as a small synchronous generator. The proposed algorithm has been tested with a 3-bus test system. Satisfactory results were obtained.

Keywords: Grid-connected photovoltaic system, Lead-acid battery, Battery Sizing, Fluctuation, Environment dependence, Copula function

1. INTRODUCTION

Due to the dramatically growth of economy and industry in recent decades, the fossil fuel consumption has been increasing considerably. However, using the fossil fuel causes many environmental problems, especially the global warming. In addition to the shortage of this kind of fuel, many countries have been awakened to resolve these problems. Natural resources, which are considered to be clean (emission free) and free of fuel expenses, are considered as the best alternative for electricity generation. The photovoltaic (PV) system, which converts solar energy to electricity, is one of those choices. Recently, large scale grid-connected PV system is more attractive in Thailand because of its cheaper development cost and high feed-in tariff offered from the government.

However, using the large scale solar PV has a major disadvantage that must be taken into account, i.e. the generated output power, voltage magnitude, and electrical frequency are fluctuated due to the intermittent solar irradiance (G) and ambient temperature ($T_{ambient}$). Dispatching these amounts of inconstant power to the utility grid will affect the quality of electricity and particularly stability of the power network. If the large PV system is connected to a weak power grid, the fluctuation may cause serious problem to the system.

Recently, there are many research works, proposed to alleviate power and frequency fluctuations caused by the PV system. Most of them aim to control behaviors of the PV system's outputs. The fuzzy logic-based control may be used to determine the number of PV modules and to control the inverter of a grid-connected PV system [1]-[3]. In addition, researchers in [4] propose the ramp rate control technique of the PV's inverter by using a shunt compensator in order to absorb or supply an insufficient power. However, these proposed techniques reduce an efficiency of the maximum power point tracking of an inverter. In practice, it has been commonly known that fluctuations of PV system's output can be reduced by three methods [5], i.e. installation of a battery storage system, use of a dump load, and curtailment of the generated PV's output power. It is essential that the PV system should feed all of generated output power into the main grid to maximize its plant factor in order to obtain the maximum revenue. Consequently, the first method sounds more logical and feasible than other methods.

Currently, there are only a few research works focused on determining the optimal size of the battery energy storage system (BESS) to reduce the power and frequency fluctuations in grid-connected PV system. Most of them concern only concepts of how to integrate the BESS to dispatch electrical power fed into the main grid [6]-[12]. In [7], a rule-based method to select the battery size is proposed. It selects the battery size from the frequency distribution of the difference between demand and output power of the PV system. In [13], the battery size is determined from the difference between daily energy demand and generated energy from the PV system. However, these proposed battery sizing methods consider only a single scenario of solar irradiance and ambient temperature. Thus, it cannot be guaranteed that the obtained battery size is truly best.

The purpose of this paper is to determine the optimal capacity of battery system to reduce fluctuations of the output power and frequency in grid-connected

Manuscript received on April 19, 2013 ; revised on June 19, 2013.

*The authors are with Department of Electrical Engineering, Faculty of Engineering, Chulalongkorn University E-mail: chattrin.th@gmail.com[1], kulyos.a@eng.chula.ac.th[2]

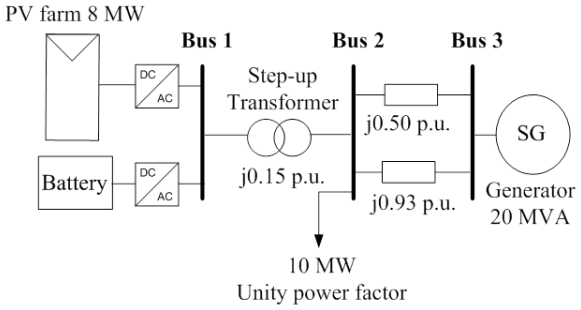

Fig.1: *Topology of photovoltaic grid connection*

mode of the PV system. The islanding mode is beyond the scope of this paper. The optimal size of the battery system should be installed into the PV system. Consequently, the battery will discharge when the PV system generates power less than the desired value. Conversely, the battery will be charged when the generated power from the PV system exceeds the set point. In this paper, all parts of the PV system, inverter, converter, as well as the BESS are thoroughly analyzed using dynamic models. Additionally, to determine the optimal battery capacity, many possible environmental conditions are taken into consideration. Thus, the obtained result is more realistic and more robust compared to previous research works. It can be said that the optimal battery capacity obtained from this proposed method enables total output of the PV system to meet the predefined set point, decrease the throughput fluctuations, and confine the total investment costs.

2. SYSTEM CONFIGURATION AND MODELING

The grid-connected PV system used in this paper can be illustrated in Fig. 1. The system consists of a PV farm with the BESS, connected to the utility grid through a step-up transformer located at bus 1. The utility grid is modeled as a synchronous generator at bus 3. A constant power load with unity power factor is located at bus 2.

Mathematical models of each part will be described in the following sequence, PV system's model, grid-connected PV model, and lead-acid battery model.

2.1 Photovoltaic System Model

2.1.1 Characteristic Equation

The five-parameter PV model used in this paper is shown in Fig. 2 [14] where I_{ph} is photoelectric current, I_d is diode current, I_{sh} is shunt resistor current, R_{sh} is shunt resistance, V_d is diode voltage, R_s is series resistance, I_{pv} is photovoltaic current and V_{PV} is terminal voltage of the PV. Diode current can be

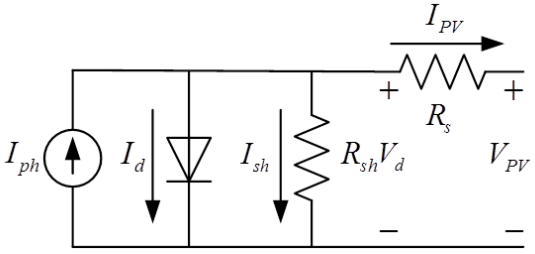

Fig.2: *Circuit diagram of PV module*

defined as

$$I_d = I_0 exp\left(\frac{V_d}{n_s V_T}\right) \tag{1}$$

where I_0 is a diode reverse saturation current, n_s is a number of series cells of module, and V_T is a thermal voltage that can be defined as

$$V_T = \frac{k_b A T_{cell}}{q} \tag{2}$$

where k_b is a Boltzmann's constant, A is an ideality factor, T_{cell} is a cell temperature and q is a coulomb constant.

By applying the Kirchhoff's current law, its current-voltage characteristic equation can be defined as

$$I_{PV} = I_{ph} = I_0\left(exp\left(\frac{V_{PV} + I_{PV}R_s}{n_s V_T}\right) - 1\right) - \frac{V_{PV} + I_{PV}R_s}{R_{sh}} \tag{3}$$

2.1.2 Dependence of the Parameters on Actual Operating Conditions

According to the I-V characteristic of PV cell, it is important to be noticed that the PV modules performance at the actual operating conditions would change from the standard test condition (STC) which is defined as the environmental condition at irradiance level (G_n) of 1000 W/m^2 with an air mass 1.5 spectrum, and at 25°C module temperature (T_{STC}). Accordingly, the PV parameters must be modified. Typically, the manufacturer datasheet provides essential parameters of the PV module at STC, such as current at the maximum power point (MPP) ($I_{mpp,n}$), voltage at MPP ($V_{mpp,n}$), short circuit current ($I_{sc,n}$), open circuit voltage ($V_{oc,n}$), thermal coefficient of the open circuit voltage (K_V), thermal coefficient of the short circuit current (K_I), nominal operating cell temperature (NOCT), number of series cells of module (n_s) and power at MPP ($P_{mpp,n}$). The five parameters at STC ($I_{ph,n}, I_{o,n}, R_{sh,n}, R_{s,n} and A_n$) can be extracted from numerical calculations using the data provided in the datasheet [14]. According to [15], the modification of these parameters should be done as follows.

$$T_{module} = T_{ambient} + \frac{(NOCT - 20)G}{0.8G_n} \tag{4}$$

$$A = \frac{A_n T_{module}}{T_{STC}} \tag{5}$$

$$V_T = \frac{Ak_b T_{module}}{q} \tag{6}$$

$$I_{sc} = \frac{I_{sc,n} G}{G_n} + K_1 \left(T_{module} - T_{STC}\right) \tag{7}$$

$$V_{oc} = V_{oc,n} + Alog\left(\frac{G}{G_n}\right) + K_V \left(T_{module} - T_{STC}\right) \tag{8}$$

$$I_{ph} = \frac{I_{ph,n} G}{G_n} \tag{9}$$

$$R_s = \frac{R_{s,n} G}{G_n} \tag{10}$$

$$R_{sh} = \frac{R_{sh,n} G}{G_n} \tag{11}$$

$$I_o = \frac{\left(I_{ph} - \frac{V_{oc}}{R_{sh}}\right)}{\left(exp\left(\frac{V_{oc}}{n_s V_T}\right) - 1\right)} \tag{12}$$

2.1.3 Photovoltaic array and its parameters

In the grid-connected PV system, only one PV module cannot provide sufficient power and voltage. Consequently, a combination of connection of these modules is required. The numbers of modules are connected in series in order to increase the voltage output of the PV system, which is called "string". These strings are connected in parallel to give a higher current output of the power source. These connections of PV module are called PV array. To simplify the model, this paper assumes that all of the PV modules have the same I-V characteristic, uniform irradiance, and unique temperature on each module.

If the PV array has the number of series-connected modules per string of N_s and the number of parallel-connected string to form an array of N_p, the modified array parameters can be calculated as follow [14].

$$V_{T,ar} = V_{T,module} \tag{13}$$

$$n_{s,ar} = n_s \times N_s \tag{14}$$

$$I_{ph,ar} = I_{ph} \times N_p \tag{15}$$

$$I_{sc,ar} = I_{sc} \times N_p \tag{16}$$

$$V_{oc,ar} = V_{oc} \times N_s \tag{17}$$

$$R_{s,ar} = R_s \times \frac{N_s}{N_p} \tag{18}$$

$$R_{sh,ar} = R_{sh} \times \frac{N_s}{N_p} \tag{19}$$

$$I_{o,ar} = I_o \times N_p \tag{20}$$

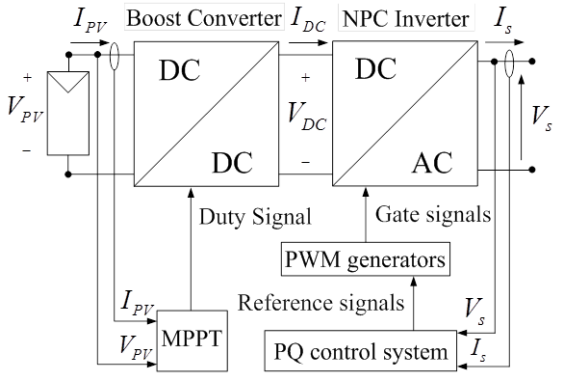

Fig.3: *Proposed grid-connected PV system structure*

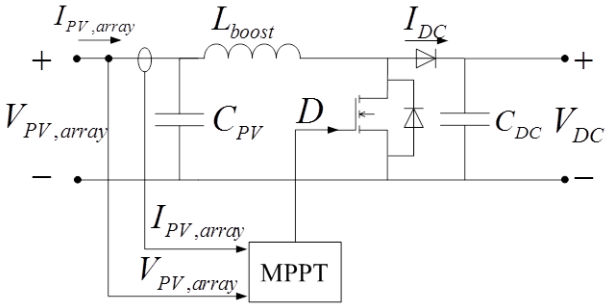

Fig.4: *Structure of the boost converter with MPPT*

2.2 Grid-connected Photovoltaic Model

The grid-connected PV system used in this paper is shown in Fig. 3 [16]. This system consists of the PV array and a double stage inverter. This inverter has two power control processes. The first one is a boost converter that is used to control the maximum power point tracking (MPPT) process. The second one is a neutral point clamp inverter (NPC). It is used to control grid current, dc-side voltage, and grid synchronization. This section is divided in two parts, i.e. the control system of boost converter and the control system of NPC inverter, respectively.

2.2.1 The Control System of Boost Converter

The structure of the boost converter shown in Fig. 4 consists of decoupling capacitor, inductor, diode, and switching. The input capacitor (C_{PV}) is used to reduce the amplitude of an array voltage ripple and eliminate the effect of switching frequency on PV array. The capacitor in the dc-link (C_{DC}) is used to decouple a voltage or frequency fluctuation between boost converter and inverter, and also to maintain constant output dc-voltage. A steady state of input voltage for boost converter can be determined as

$$V_{PV,ar} = V_{DC}(1 - D) \tag{21}$$

where $V_{PV,ar}$ is a PV array voltage, V_{DC} is an output voltage, and D is a duty ratio.

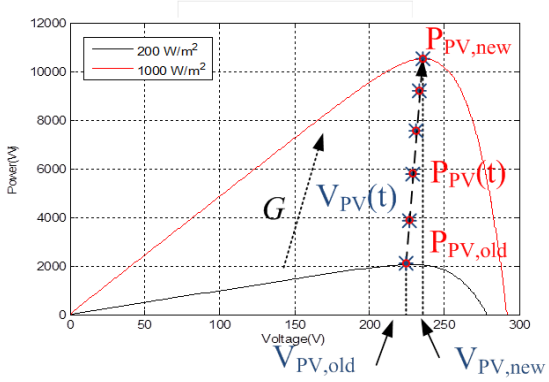

Fig.5: *The P&O operating point path of rapid change in irradiation level.*

2.2..1.a Maximum Power Point Tracking (MPPT)

Perturb and observe algorithm is the most widely used method of MPPT due to the simplicity and robustness [17]. This method controls the amplitude of duty cycle that leads to adjustments of the array voltage around the MPP as shown as follows.

$$D\left((k+1)T_a\right) = D\left(kT_a\right) + \Delta d \times sign(\Delta P_{PV}) \quad (22)$$

$$\Delta d = \left|D(kT_a) - D\left((k-1)T_a\right)\right| \quad (23)$$

$$\Delta P_{PV} = P_{PV}(kT_a) - P_{PV}((k-1)T_a) \quad (24)$$

A next duty cycle at the $k+1$ is determined based on ΔP_{PV} and Δd. The sign of perturbation depends on the difference of sampling output power. The MPPT senses array voltage and current every T_a second. According to this principle, the extracted power will oscillate around the actual maximum power point. Moreover, the optimal value of disturbance Δd and time duration T_a is required to provide high efficiency of power extraction [18].

An example of MPPT is shown in Fig. 5. The rapid change of irradiation level leads to change of the operating point of PV array. The P&O-MPPT tracks the instantaneous maximum power until the tracker meets a final value. After that, if environment conditions are maintain a constant, the tracker will controls an operating point oscillating around real MPP.

2.2.1.b Dynamics Characteristic of DC to DC Boost Converter

Instantaneous mode of array voltage can be expressed asInstantaneous mode of array voltage can be expressed as

$$V_{PV}(t) = V_{MPP}(t) + \Delta v_{PV}(t) \quad (25)$$

where $V_{MPP}(t)$ is the instantaneous array voltage at MPP and $\Delta v_{PV}(t)$ is the variation of array voltage.

By using the small signal analysis to the converter, the variation of the PV array voltage can be defined as

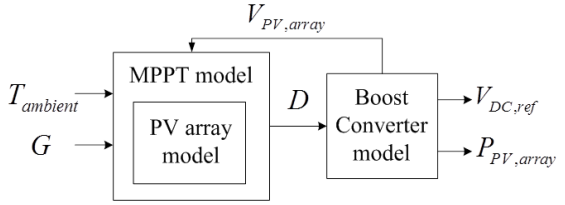

Fig.6: *Schematic diagram of boost converter control*

$$\widehat{V}_{PV} = G_{vd}(s)\Delta d(s) + G_{vload}(s)i_{load}(s) \quad (26)$$

where G_{vd} is the duty cycle perturbation to array voltage transfer function and G_{vload} is the load to array voltage transfer function. The detail of both transfer functions are shown in (27) and (28) respectively.

$$G_{vd}(s) = \frac{-V_{DC}}{L_{boost}C_{PV}s^2 + \left(\frac{L_{boost}}{R_{load}(1-D_k)^2}\right)s + 1} \quad (27)$$

$$G_{vload}(s) = \frac{-R_{load}(1-D_k)}{As^3 + Bs^2 + Cs + 2} \quad (28)$$

for an ideal boost converter

$$R_{load} = \frac{R_{MPP}(t)}{(1-D_k)^2} \quad (29)$$

$$i_{load}(s) = \frac{V_{DC}(s)(1-D_k)^2}{R_{MPP}(t)} \quad (30)$$

where A, B and C are

$$A = L_{boost}C_{PV}R_{load}C_{DC} \quad (31)$$

$$B = \left(C_{PV} + \frac{C_{DC}}{(1-D_k)^2}\right)L_{boost} \quad (32)$$

$$C = R_{load}(C_{PV}(1-D_k)^2 + C_{dc}) + \left(\frac{L_{boost}}{R_{load}(1-D_k)^2}\right) \quad (33)$$

2.2.2 The Control System of NPC Inverter

A single phase three level voltage source inverter (VSI) is shown in Fig. 8. It composes of diodes and switching. The total switching loss and on-stage loss represent as R_P and R respectively. An inductor L represents the total inductance of an ac filter and a cable. The terminal of NPC is connected to the power grid.

By the generalized state-space averaging method proposed in [19], the NPC model can be simplified. In this section, the control functions of NPC are divided into two control parts, i.e. grid current and dc-side voltage.

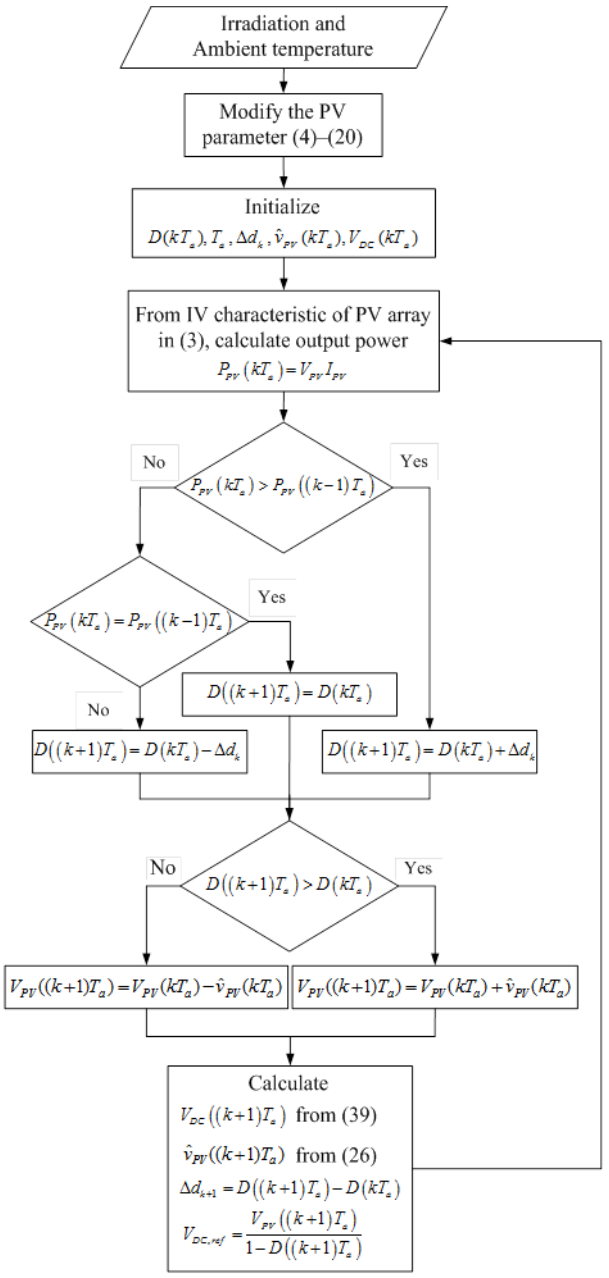

Fig.7: *Flowchart diagram of MPPT*

2.2.2.a Grid Current Control

An inverter controls direct and quadrature axes of the grid current on the synchronous reference frame (i_{sd} and i_{sq} respectively) [20]. The time constant (τ_i) of this process is about 5 to 50 ms.

$$\frac{di_{sd}}{dt} = \frac{-i_{sd}}{\tau_i} + \frac{i_{sd,ref}}{\tau_i} \tag{34}$$

$$\frac{di_{sq}}{dt} = \frac{-i_{sq}}{\tau_i} + \frac{i_{sq,ref}}{\tau_i} \tag{35}$$

2.2.2.b DC-link Voltage Control

The fundamental of dc-voltage control is the balance of and electrical power transfer between dc and ac side. The reference current on direct axis from previous section can be calculated through this control. Moreover, the feed forward compensation is needed to control grid current and voltage at point of common coupling (PCC) in order to reduce the loss effect of an inverter. The simplified control model follows in [19]. Consequently, the reference direct axis current can be shown as

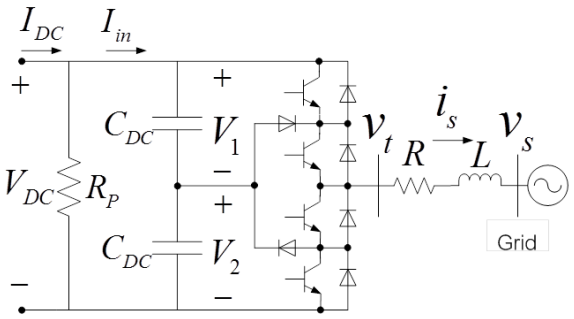

Fig.8: *Structure of three-level NPC inverter*

$$i_{sd,ref}(t) = \alpha_2 x_1 + \alpha_1 x_2 + \frac{2P_{PV,ar}(t)}{3V_{sd}(t)} \tag{36}$$

where x_1 and x_2 are defined as

$$\frac{dx_1}{dt} = x_2 \tag{37}$$

$$\frac{dx_2}{dt} = \alpha_3 x_2 - V_{DC}^2 + V_{DC,ref}^2 \tag{38}$$

The state equations of dc-link control can be shown as

$$\begin{aligned}\frac{C_{eq}}{2}\frac{dV_{DC}^2}{dt} = V_{DC}I_{DC} - \frac{V_{DC}^2}{R_p} - \frac{3}{4}\frac{d\left(Li_{sd}^2 + Li^2sq\right)}{dt} \\ -\frac{3}{2}R\left(i_{sd}^2 + i_{sq}^2\right) - \frac{3}{2}\left(v_{sd}i_{sd}^2 + v_{sq}i_{sq}^2\right)\end{aligned} \tag{39}$$

where α_1, α_2 and α_3 are control parameter of PI controller. C_{eq} equals $C_{DC}/2$. $i_{sd,ref}$ is a reference direct axis current. $V_{DC,ref}$ is a reference dc-link voltage. v_{sd} and v_{sq} are direct axis and quadrature axis grid voltage respectively.

2.3 Lead-acid Battery Model

A lead-acid battery is used in this paper. The mathematical model of lead battery represented in charge and discharge modes can be shown as follows [21].

$$V_{b,ch} = E_o - R_b i - K\left(\frac{Qi^*}{Q_t + 0.1Q} - \frac{QQ_t}{Q - Q_t}\right) + Exp(t) \tag{40}$$

$$V_{b,dch} = E_o - R_b i - K\frac{Q}{Q - Q_t}(Q_t + i^*) + Exp(t) \tag{41}$$

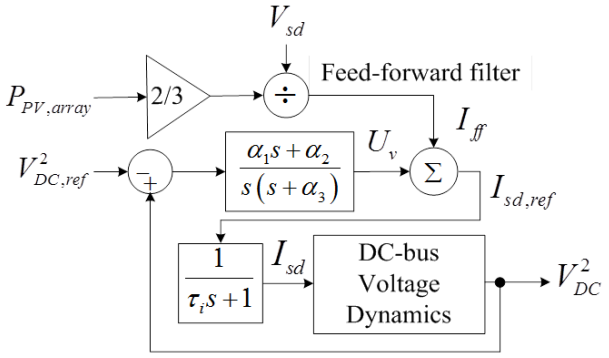

Fig.9: *Schematic diagram of active power control*

$$\frac{dExp(t)}{dt} = \tau_{exp} \cdot |i(t)| \cdot (-Exp(t) + V_{exp}u(t)) \quad (42)$$

$$Q_t = \int_0^{\Delta t} i(t)dt \quad (43)$$

where E_o is a battery constant voltage, R_b is an internal resistance, K is a polarization resistance and Q is a nominal battery capacity. Q_t is an extracted or corrected charge at time interval Δt. Both current i and filtered current i^* will be positive if battery is in discharge mode and vice versa. The exponential zone voltage $Exp(t)$ represents in (42) depends on time constant inverse (τ_{exp}), exponential zone amplitude (V_{exp}) and charge ($u(t) = 1$) or discharge ($u(t) = 0$) mode.

3. SOLAR IRRADIATION AND AMBIENT TEMPERATURE MODELS

The stochastic models describing solar intensity and ambient temperature as a Brownian motion can be shown in (44)-(45).

$$G_t = G_{avg,i} exp\left(\sigma_{G,i} Z_{G,i}\sqrt{t} - \frac{t\sigma^2_{G,i}}{2}\right) \quad (44)$$

$$T_{ambient,t} = T_{avg,i} exp\left(\sigma_{T,i} Z_{T,i}\sqrt{t} - \frac{t\sigma^2_{T,i}}{2}\right) \quad (45)$$

where G_t is an irradiance at time t of hour $i, G_{avg,i}$ is an average irradiance at hour $i, \sigma_{G,i}$ is a variance of G at hour $i, Z_{G,i}$ is a normally distributed random number describing G at hour i and t is a sampling time interval. $T_{ambient,t}$ is an ambient temperature at time t of hour i, $T_{avg,i}$ is an average temperature at hour $i, \sigma_{T,i}$ is a variance of $T_{ambient}$ at hour $i, Z_{T,i}$ is a normally distributed random number describing $T_{ambient}$ at hour i.

However, in fact, solar irradiance and ambient temperature have some relationship. A day with high solar irradiance comes with high ambient temperature. Conversely, low solar irradiance comes with low ambient temperature. Consequently, the dependence between irradiation and ambient temperature should be taken into account in determining the output power of the PV array.

Copula is a mathematical theory that can describe the relationship between random variables in the form of joint cumulative distribution function (joint cdf). Sklar's theorem is the main principle in copula analysis. It states that H is a joint cdf of two random variables if it has a copula C such that [22]

$$H(x, y) = C(F(x), G(y)) \quad (46)$$

where $x, y \in R.F(x)$ and $G(y)$ are the marginal cumulative distribution of x and y, respectively.

Thus, correlation between (44) and (45) can be determined from (46) with the joint cdf of $Z_{G,i}$ and $Z_{T,i}$ depending on an appropriate standard copulas, e.g. Clayton, Flank, or Gumbel copulas.

4. DETERMINING THE OPTIMAL BATTERY CAPACITY

A required capacity of battery energy storage system (BESS) can be calculated by power flowing into or out of the battery that is expressed by

$$P_{batt,t} = P_{set} - P_{PV,t} \quad (47)$$

where P_{set} is a set point power that is required to feed into the grid. If $P_{batt,t} > 0$, the battery will discharge. On the other hand, if $P_{batt,t} < 0$, the battery will be charged. The optimal capacity of battery in each time interval can be determined from

$$Q_{opt.t} = \begin{cases} |P_{batt}| \frac{Q}{V_{b,dch} i_{batt,max}}, P_{batt} > 0 \\ |P_{batt}| \frac{Q}{V_{b,ch} i_{batt,max}}, P_{batt} > 0 \end{cases} \quad (48)$$

where Q is a nominal capacity of a single battery, $i_{batt,max}$ is the maximum charging current of a single battery, determined from the minimum between battery's maximum charging current and inverter's rated current.

Many environmental conditions are taken into account when determining the required battery capacity. Finally, $Q_{opt,t}$ is determined from the 95th percentile of all occurrences of battery sizes that the battery would support the PV system to maintain constant output power.

5. NUMERICAL EXAMPLE

5.1 Example of Irradiance and Ambient Temperature Sampling

The mean and standard deviation of hourly irradiance and ambient temperature used in this example can be shown in Table 1. By using (44) - (46), both solar irradiance and ambient temperature are sampled. Fig. 10 illustrates the sample of irradiance and ambient temperature in one day on rainy season by using the sampling time interval of 1/360 hours. The result shows that solar irradiance and ambient temperature vary around the average values.

Table 1: *The average and variation of irradiation and ambient temperature in rainy season*

Time	G_{avg} (W/m^2)	σ_G	T_{avg} $(^\circ C)$	σ_T
7-8	131.62	0.9599	2.14	0.0431
8-9	288.10	0.7154	26.29	0.0523
9-10	473.29	0.6271	27.38	0.0596
10.11	613.53	0.4522	28.55	0.0658
11-12	732.30	0.3887	29.62	0.0685
12-13	722.82	0.6614	30.33	0.0703
13-14	656.90	0.5861	30.71	0.0739
14-15	595.83	0.6378	30.87	0.0797
15-16	494.55	0.5114	30.91	0.0837
16-17	366.11	0.5434	30.73	0.0778
17-18	192.90	0.6477	30.08	0.0765

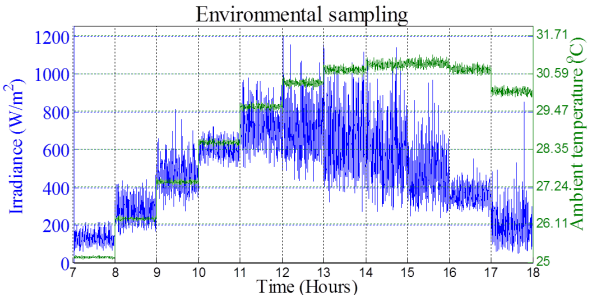

Fig.10: *One day sampling of solar irradiance and ambient temperature in rainy season.*

5.2 Example of Generated Power and Frequency Sampling before Installation the Battery

The photovoltaic system parameters used in this paper are shown in Table 3. The initial PV system control parameters are shown in table 4. In addition, parameters of the 4-state generator model representing the rest of the power grid [23] are shown in Table 5. This paper uses 48,240 modules of KC175GH for 8 MW installations [24]. The five-parameter of this PV module is shown in Table 2. When the solar irradiance and ambient temperature have been simulated, the output power of PV array can be calculated from the equations described in section 2. After that, the inverter extracts the maximum power from PV based on the MPPT control principles described in Fig.7. Simultaneously, it converts the DC electricity to the AC electricity by the NPC inverter control described in the section 2.2.2.

By using the PV system parameters shown in Table 3 and the initial PV system control parameters shown in Table 4, the output power of PV system can be shown in Fig 11. It is obviously seen that the fluctuation of output power has an impact on the system frequency so that the frequency deviates from the allowed range of 49.5 to 50.5 Hz. as shown in Fig. 12.

Table 2: *Photovoltaic module parameters*

Parameter	Value	Unit
$I_{ph,n}$	8.0926	A
$I_{o,n}$	1.1693	μA
$R_{s,n}$	0.106	Ω
$R_{sh,n}$	325.5401	Ω
$V_{T,n}$	0.0387	V

Table 3: *Photovoltaic system parameters*

Parameter	Value	Unit
C_{pv}	2	mF
L_{boost}	10	mH
C_{DC}	25	mF
R_p	25	$k\Omega$
R	3.5	$m\Omega$
L	3	mH
$V_{inverter}$	416	V_{L-L}
V_{base}	22	kV_{L-L}
S_{base}	20	MVA
Inverter	67	Unit
MPPT/inverter	12	Unit
N_s/MPPT	10	Unit
N_p/MPPT	6	Unit

5.3 Example of Battery Capacity Determination

Although total capacity of the PV system used in this paper is 8 MW, the daily average output power generated from the PV system is approximately only 3.5 to 4 MW. Thus, this example establishes the set point of desired output power of the PV system (P_{set}) at 4 MW.

This paper uses the S12-290AGM - 12 Vdc, 260 Ah lead acid battery [25] and the AT30 SERIES - 130Vdc charger [26] for the BESS system. The battery parameters are shown in Table 6. According to the manufacturer data sheet, the maximum charging current, $i_{batt,max}$, is 50 A. In addition, the parameters of DC-AC charger in the BESS system are exactly the same as the parameter of DC-AC inverter in the PV system.

In this paper, the capacity of the battery is selected such that it can cover 95% of all possible occurrences in one-year sampling environmental data. That means it covers all three-season behaviours, i.e. summer, rainy, and winter. From the example in Fig 13, the calculated battery capacity is 1.6134 MAh. However, this calculated battery capacity corresponds with only one case of data sampling in a year, so it cannot represent the best choice of the optimal battery capacity. Therefore, 1,000 scenarios are generated using the same hourly solar irradiance and ambient temperature data. By applying the same method to determine the optimal battery capacity of

Table 4: *Photovoltaic system parameters*

Parameter	Value	Unit
$V_{PV,0}$	$0.9V_{oc,array}$	V
$P_{PV,0}$	0	W
D_0	0.4-0.4	-
$V_{DC,0}$	600	V
$i_{d,0}, i_{q,0}$	0	A
$x_{1,0}, x_{2,0}$	0	-
$i_{sq,ref}$	0	A
Δd	0.01	-
T_a	1	s
τ_i	5	ms
α_1	-1	-
α_2	-5	-
α_3	1000	-

Table 5: *Photovoltaic system parameters*

Parameter	Value	Unit
H	1	s
X_d	1.1	pu
X_q	0.65	pu
$X_d^{'}$	0.26	pu
$X_q^{'}$	0.13	pu
$T_{do}^{'}$	7	s
$T_{qo}^{'}$	1	s

Table 6: *Photovoltaic system parameters*

Parameter	Value	Unit
E_0	12.4526	V
R_b	0.0018	Ω
K	0.0016	Ω
V_{exp}	0.1408	V
τ_{exp}	0.3297	A/h

each scenario, 1000 battery capacities corresponding to each set of sampled data can be obtained. The optimal battery capacity from 1,000 scenarios presented as a frequency distribution curve, which represents a probability density function, can be depicted in Fig. 14. With 95% of confidence interval of the probability density function, the optimal battery capacity lies between 1.6086 MAh and 1.6250 MAh. After the optimal battery capacity interval is calculated, the number of battery for series and parallel connections must be determined to match the required battery voltage and total optimal capacity. From the specifications of the lead-acid battery and the charger described above, 10 batteries must be connected in series in order to generate the specified voltage level, approximately 130 Vdc, for the inverter. Then, 625 battery strings must be connected in parallel to obtain the battery size of 1.6250 MAh. As a result, one set of BESS consists of 6,250 batteries.

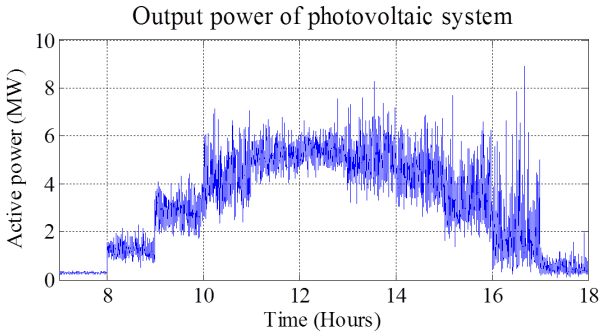

Fig. 11: *Active power sampling of photovoltaic system*

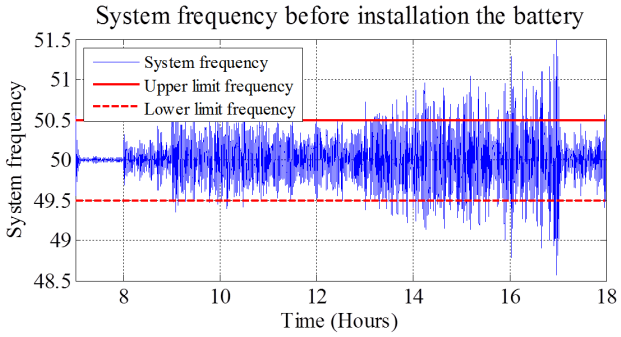

Fig. 12: *System frequency before installation the battery*

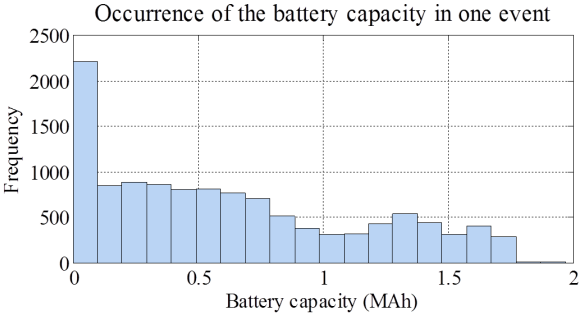

Fig. 13: *Frequency distribution of battery size of one sampling data*

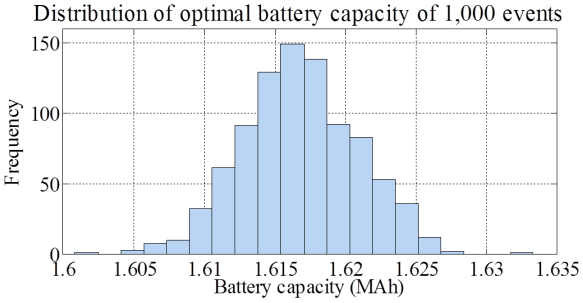

Fig. 14: *Frequency distribution of 1,000 battery sizes*

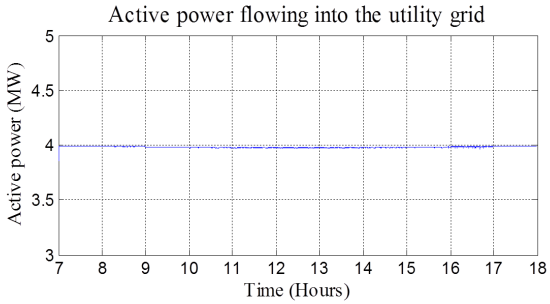

Fig.15: Test result of active power flowing into the grid

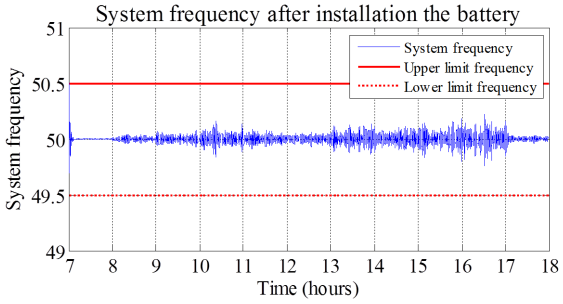

Fig.16: System frequency after installation the battery

5.4 Test Result of Power Flowing into the Utility Grid and the System Frequency after Installation the Optimal Battery Size.

To illustrate that the designed battery capacity can mitigate fluctuations of the generated output power, and system frequency, the designed battery system is then equipped with the PV system. The output power of this PV generation system with battery (P_{set}) is set to 4 MW, equal to the earlier P_{set} used in the process of battery capacity calculation. Afterward, a set of environmental conditions is sampled. Then, power flow calculations of the PV system with the BESS are analyzed. The simulation results are illustrated in Fig. 15 and 16.

The BESS determined from the proposed method contains 625 battery strings connected in parallel. Each string comprises 10 batteries connected in series. The capacity of each single battery is 260 Ah. The nominal DC voltage of each battery is 12 V. The maximum charge current is 50 A/string. Hence, the optimal capacity of this BESS is 1.625 MAh, 3.75 MW. It is 93.75% compared to the set point of this PV system output, which is 4 MW. In addition, it is 37.5% compared to the system peak demand of 10 MW.

It can be seen from Fig. 15 that installation of the optimal battery capacity determined from the proposed method can reduce the power fluctuation of the PV system and can maintain constant power flowing into the utility's grid. In addition, system frequency fluctuation can also be reduced. It is obviously seen that system frequency varies within the allowed frequency limit as shown in Fig. 16.

6. CONCLUSIONS

This paper proposes a method to determine the optimal battery capacity with a lead-acid battery dynamic model. Installing the optimal battery capacity in the system can alleviate the inconsistent output power and frequency problems that may lead to grid instability.

It is obviously seen that the total generated output power and frequency resulted from the experiment has satisfactorily less fluctuation. The fluctuation of the generated power can be noticeably alleviated by installing the battery, with the capacity chosen from the proposed method.

References

[1] M. Datta, T. Senjyu, A. Yona, T. Funabashi and C. H. Kim, "A coordinated control method for levelling PV output power fluctuations of PV-diesel hybrid systems connected to isolated power utility" *IEEE Trans. Energy Convers.*, vol. 24, no. 1, pp. 153-162, Mar. 2009.

[2] T. Senjyu, M. Datta, A. Yona, H. Sekine, and T. Funabashi, "A new method for smoothing output power fluctuations of PV system connected to small power utility," *The 7th Int. Conf. Power Electron.*, pp. 829-834, Oct. 2007.

[3] T. Senjyu, M. Datta, A. Yona, and C. H. Kim, "A control method for small utility connected large PV system to reduce frequency deviation using a minimal-order observer," *IEEE Trans. Energy Convers.*,vol. 24, no. 2, pp. 520-528, Jun. 2009.

[4] N. Kakimoto, H. Satoh, S. Takayama, and K. Nakamura, "Ramp-rate control of photovoltaic generator with electric double-layer capacitor," *IEEE Trans. Energy Convers.*, vol. 24, no. 2, pp. 465-473, Jun. 2009.

[5] W. A. Omran, M. Kazerani, and M. M. A. Salama, "Investigation of methods for reduction of power fluctuations generated from large grid-connected photovoltaic systems," *IEEE Trans. Energy Convers.*, vol. 26, no. 1, pp. 318-327, Mar. 2011.

[6] H. Fakham, D. Lu and B. Francois, "Power control design of a battery charger in a hybrid active PV generator for load-following applications,"*IEEE Trans. Indu. Elect.*, vol. 58, no. 1, pp. 85-94, Jan. 2011.

[7] S. Teleke, M. E. Baran, S. Bhattacharya, and A. Q. Huang, "Rule-based control of battery energy storage for dispatching intermittent renewable sources," *IEEE Trans. Sustainable Energy*, vol. 1, no. 3, pp. 117-124, Oct. 2010.

[8] Y. Riffonneau, S. Bacha, F. Barruel, and S. Ploix, "Optimal power flow management for grid connected PV systems with batteries," *IEEE Trans. Sustainable Energy*, vol. 2, no. 3, pp. 309-320, Jul. 2011.

[9] B. Lu, and M. Shahidehpour, "Short-term scheduling of battery in a grid-connected PV/battery system," *IEEE Trans. Power Syst.*, vol. 20, no. 2, pp. 1053-1061, May 2005.

[10] K. C. Marwali, H. Ma, S. M. Shahidehpour, and K. H. Abdul-Rahman, "Short term generation scheduling in photovoltaic-utility grid with battery storage," *IEEE Trans. Power Syst.*, vol. 13, no. 3, pp. 1057-1062, Aug. 1998.

[11] S. J. Chiang, K. T.Chang, and C. Y. Yen, "Residential photovoltaic energy storage system," *IEEE Trans. Indu. Elect.*, vol. 45, no. 3, pp. 385-394, Jun. 1998.

[12] M. Datta, T. Senjyu, A. Yona, T. Funabashi and, C. H. Kim, "A frequency-control approach by photovoltaic generator in a PV-diesel hybrid power system," *IEEE Trans. Energy Convers.*, vol. 26, no. 2, pp. 559-571, Jun. 2011.

[13] C. Venu, Y. Riffonneau, S. Bacha, and Y. Baghzouz, "Battery storage system sizing in distribution feeders with distributed photovoltaic systems," *PowerTech, 2009 IEEE Bucharest*,pp. 1-5, Jul. 2011.

[14] A. Chatterjee, A. Keyhani, and D Kapoor, "Identification of photovoltaic source models," *IEEE Trans. Energy Convers.*, vol. 26, no. 3, pp. 883-889, Sept. 2011.

[15] A. Choufer, S. Silvestre, N. Sadaoui, and L. Rahmani, "Modeling and simulation of a grid connected PV system based on the evaluation of main PV module parameters," *Simulation Modeling Practice and Theory*, vol. 20, iss. 1, pp. 46-58, Jan 2011.

[16] S. B. Kjaer , J. K. Pedersen, and F. Blaabjerg "A Review of single-phase grid-connected inverters for photovoltaic modules," *IEEE Trans. Indu. Appl.*, vol. 41, no. 5, pp. 1292-1306, Sept. 2005.

[17] T. Esram, and P. L. Chapman, "Comparison of photovoltaic array maximum power point tracking techniques," *IEEE Trans. Energy Convers.*, vol. 22, no. 2,pp. 439-449, Jun. 2007.

[18] N. Femia, G. Petrone, G. Spagnuolo, and M. Vitelli,"Optimization of perturb and observe maximum power point tracking method," *IEEE Trans. Power Electron.*, vol. 20, no. 4, pp. 963-973, Jul. 2005.

[19] A. Yazdani, and R. Iravani, "An accurate model for the DC-side voltage control of the neutral point diode clamped converter," *IEEE Trans. Power Deliv.*, vol. 21, no. 1, pp. 185-193, Jan. 2006.

[20] R. Teodorescu, M. Liserre, and P. Rodriguez, "Grid converters for photovoltaic and wind power systems," United Kingdom: John Wiley & Sons, 2011.

[21] O. Tremblay, and L. A. Dessaint, "Experimental validation of a battery dynamic model for EV applications," *World Electric Vehicle J.*, vol. 3, 2009.

[22] U. Cherubini, E. Luciano and W. Vecchiato, "Copula methods in finance," United Kingdom: John Wiley & Sons, 2004.

[23] Kundur P., *Power System Stability and Control,* McGraw-Hill, 1994.

[24] Kyocera Solar Inc. *KC175GHT-2 datasheet.* [Online]. available :http:// www.kyocerasolar.eu

[25] ROLLS BATTERY Ltd. *S12-290AGM datasheet.* [Online]. available :http://www.rolls-battery.com

[26] Hindle Power Inc. *AT30 SERIES 130Vdc datasheet.* [Online]. available : http://www.hindlepowerinc.com

Chattrin Thongsawaeng received the B.Eng from Chulalongkorn University, Thailand in 2011. At present, he is pursuing the M.Eng at Chulalongkorn University. He is interested in renewable energy.

Kulyos Audomvongseree received the B.Eng and M.Eng from Chulalongkorn University, Thailand, in 1998 and 2000 respectively. He obtained a Ph.D from University of Tokyo, Japan, in 2004. He also received the M.Sc. Finance from Thammasat Business School, Thailand, in 2010. He is now an assistant professor at the faculty of Engineering, Chulalongkorn University.